Contribution of Oceanic Gas Hydrate Dissociation to the Formation of Arctic Ocean Methane Plumes

Matthew T. Reagan[1]
George J. Moridis[1]
Scott M. Elliott[2]
Mathew Maltrud[2]

[1]Lawrence Berkeley National Laboratory
1 Cyclotron Rd. Berkeley, CA 94720 USA

[2]Los Alamos National Laboratory
P.O. Box 1663, Los Alamos, NM 87545 USA

e-mail: MTReagan@lbl.gov

ABSTRACT

Vast quantities of methane are trapped in oceanic hydrate deposits, and there is concern that a rise in the ocean temperature will induce dissociation of these hydrate accumulations, potentially releasing large amounts of carbon into the atmosphere. Because methane is a powerful greenhouse gas, such a release could have dramatic climatic consequences. The recent discovery of active methane gas venting along the landward limit of the gas hydrate stability zone (GHSZ) on the shallow continental slope (150 m - 400 m) west of Svalbard suggests that this process may already have begun, but the source of the methane has not yet been determined. This study performs 2-D simulations of hydrate dissociation in conditions representative of the Arctic Ocean margin to assess whether such hydrates could contribute to the observed gas release. The results show that shallow, low-saturation hydrate deposits, if subjected to recently observed or future predicted temperature changes at the seafloor, can release quantities of methane at the magnitudes similar to what has been observed, and that the releases will be localized near the landward limit of the GHSZ. Both gradual and rapid warming is simulated, along with a parametric sensitivity analysis, and localized gas release is observed for most of the cases. These results resemble the recently published observations and strongly suggest that hydrate dissociation and methane release as a result of climate change may be a real phenomenon, that it could occur on decadal timescales, and that it already may be occurring.

Index Terms: 1605, 1635, 1807, 1847, Keywords: gas hydrates, climate change

1. INTRODUCTION

Gas hydrates are solid crystalline compounds in which gas molecules are lodged within the clathrate crystal lattice (Sloan and Koh, 2008). Natural gas hydrate deposits occur in geologic settings where the necessary low temperatures and high pressures exist for their formation and

stability. Vast quantities of methane are trapped in oceanic hydrate deposits. Because methane is a powerful greenhouse gas (about 26 times more effective than CO_2), there is considerable concern that a rise in the ocean temperature will induce dissociation of these hydrates, potentially releasing large amounts of carbon into the atmosphere.

Initial investigations estimated the total amount of methane hydrate currently residing in the deep ocean and along continental margins, beginning with an early "consensus value" of 10,000 gigatons (Gt, 20×10^{15} m^3 STP) of methane carbon (Gornitz and Fung, 1994; Kvenvolden, 1999; Borowski, 2004). However, more recent studies have produced widely different results—one yielding an upper estimate of 27,300 Gt of methane in hydrate along continental margins (74,400 Gt globally) (Klauda and Sandler, 2005) while others a much lower estimate of 3,000 Gt of methane in hydrate (Buffett and Archer, 2004) or even less than 300 Gt under restrictive formation regimes (Archer et al., 2009). Regardless of the total volumes involved, biogenic methane production, and hence the expected existence of hydrate, is particularly significant in arctic waters along the continental margin (Archer et al., 2009).

In oceanic deposits, the depth at which hydrates remain stable depends on the pressure (as imposed by the water depth) and the temperature. An increase in water temperature at the seafloor changes the extent of the gas hydrate stability zone (GHSZ), and such a shift could induce hydrate dissociation and lead to methane release. Deep ocean surveys have found pockmarks and other structures that indicate violent fluid releases at the seafloor in the past (Hovland et al., 2005), and computational studies show potential hydrate instability during warming (Reagan and Moridis, 2008).

Such releases could have dramatic climatic consequences because they could amplify atmospheric and oceanic warming and possibly accelerate dissociation of remaining hydrates. This positive-feedback mechanism has been proposed as a significant contributor to rapid and significant climate changes in the late Quaternary period (Kennett et al., 2000). The Clathrate Gun Hypothesis (Kennett et al., 2002) proposes that past increases in water temperatures near the seafloor may have induced such a large-scale dissociation, with the methane spikes and isotopic anomalies reflected in polar ice cores and in benthic foraminifera. While this hypothesis is controversial, and relationships between hydrates and climate have not yet been established, the role of methane in climate cycles is currently an active area of research and hydrates are considered to be a potential source (Mascarelli, 2009).

The recent discovery of active gas venting along the shallow continental slope west of Svalbard creates new cause for concern (Westbrook et al., 2009). Over 250 plumes were observed in water depths shallower than 400 m. The observed plumes release a sizeable quantity of methane—with some plumes extending to within 50 m of the sea surface. Seismic sections indicated rising gas in the sediments and free gas below the GHSZ. While methane seeps are known to exist in other locations, this system is notable in that the locations of the plumes coincide with the landward limit of the GHSZ, suggesting that recent changes in seafloor temperature have interacted with shallow hydrates in the subsurface (Reagan and Moridis, 2009). Two hydrate-related phenomena are proposed: 1) that dissociating shallow hydrates are responsible for the methane and 2) that methane arriving from deeper sources forms hydrate in the shallow GHSZ, and this hydrate (due to the change in effective permeability) may act to block or channel methane that migrates upward from deeper sources. To test this hypothesis, this study performs large-scale, 2-D simulations of shallow hydrates in conditions representative of

the western Svalbard margin to assess the potential for hydrate dissociation, methane release, and methane plume formation in arctic continental shelf environments subjected to ocean warming.

2. MODELS AND METHODS

We evaluate the stability and dissociation of shallow oceanic hydrates subjected to short-term temperature variations and the flow of methane in the subsurface using the massively parallel version of the TOUGH+HYDRATE code (pT+H) (Moridis et al., 2008). T+H models the nonisothermal hydration reaction, phase behavior and flow of fluids and heat in complex geologic media (Moridis and Kowalsky, 2007; Moridis and Sloan, 2007) and has been used in earlier 1-D studies of hydrate dissociation in response to ocean temperature change (Reagan and Moridis, 2008). This study is the first simulation of fully coupled hydrate dissociation, heat transport, and multiphase flow applied to a climate-driven system of this magnitude.

2.1 Domain Discretization and Initial Configuration

The model is a 2-D sloping system 5000 m in length and extending to 300 m below the seafloor. The western Svalbard continental shelf has a 3%-5% slope, as indicated by averages from GEBCO bathymetry data for the western Svalbard region (GEBCO, 1997) and as reported by Westbrook et al. (2009) in the region of methane plume formation. We initially select a 5% grade (20 m per 1 m depth) to constrain the horizontal extent of the system. The top of the slope is located at a depth of 300 m, above the top of the GHSZ at local temperatures, with the bottom of the slope at 550 m at a 5% grade. Figure 1 shows a schematic of the mesh (not to scale), including the system boundaries and the extent of the GHSZ. To represent the system at a suitable level of detail, we use 300,000 gridblocks (1000 x 300), with a horizontal discretization of dx = 5 m, a 2-D slice thickness of dy = 1 m, and a variable vertical discretization, beginning

with dz = 0.25 m from the seafloor to z = -50 m, dz = 0.5 m between z = -50 m and z = -75 m, and a logarithmic progression (dz = 0.5 – 15.8m) from z = -75 to z = -300 m.

The initial condition for the Base Cases involve a hydrostatic pressure distribution based on depth and 3.5 wt% salinity, initial temperature based on a geothermal gradient of 8.7 ˚C/100 m (Haacke et al., 2008) extrapolated from surface measurements, and a uniform initial hydrate saturation of 3% in the sediment column within the GHSZ. The extent of the GHSZ is computed directly from the depth and initial temperature using T+H (Moridis, 2003; Moridis et al., 2008). The temperature and pressure profiles, heat flow through the sediments, and equilibrium distribution of hydrate and dissolved methane in the aqueous phase are derived from simulations, and the each initial condition is brought to thermal, hydrostatic, and chemical equilibrium. A preexisting region of free gas, often inferred to exist underneath shallow stratigraphic hydrate deposits, is not included in this simulation, as the actual quantity of gas under systems of this type has not been directly measured and our goal is to assess the quantity of gas that may be released due to hydrate dissociation alone.

2.2 System Properties

The intrinsic permeability for the Base Cases, k = 1 mD, is within the reported range of hydrate-bearing oceanic sediments (Ginsberg and Soloviev, 1998) and represents a baseline stratigraphic or “Class 4” hydrate deposit (Moridis and Sloan, 2007), in contrast to the less common, more permeable, and often more saturated structural deposits near sites of active methane seepage and/or venting. The porosity φ = 0.55 reflects measurements taken at deeper locations further offshore (Haake et al., 2008). The physical properties parameters used in the simulations are summarized in Table 1.

The top of the sediment column is bounded by an open boundary representing heat and mass transfer between the sediment and the bulk ocean. The pressure at the upper boundary (set according to hydrostatic conditions at the initial salinity) is held constant, representing constant ocean levels. The bottom of the domain is a closed boundary at z = -300 m, beyond the expected range of temperature propagation on short timescales, and is held at a constant temperature selected to match the desired initial geothermal gradient and supply the geological heat flux from an infinitely thick underburden.

2.3 Climate Change Scenarios

Recent climate simulations coupling ocean circulation, atmospheric circulation, and atmospheric chemistry (Meehl et al., 2007) indicate that, under current climate conditions and a 1%/yr increase in atmospheric CO_2, the temperature at the seafloor would rise by 1 ˚C over the next 100 yr, and possibly by another 3 ˚C in the following century. Historical temperature data from the Svalbard region (Westbrook et al., 2009) suggest that a 1 ˚C change in bottom-water temperature has already occurred over the last 30 years. Previous work on the response of shallow hydrates to ocean temperature change (Reagan and Moridis, 2008) indicates that temperature changes as small as 1 – 3 ˚C can have significant effects on shallow hydrates.

2.4 Base Cases

For the Base Cases, we use the homogeneous initial conditions described in the previous section, and vary the temperature at the upper boundary to represent these changes in the bulk ocean temperature above the seafloor. For all simulations, we assume an initial seafloor

temperature of T_0 = 0 ˚C (Westbrook et al., 2009). For Base Case I, we increase the overlying ocean temperature by 1 ˚C/100 yr, a conservative representation of possible temperature changes over the last century, and also a conservative projection of potential warming in the near future. We simulate the evolution of the system for a total of 300 yr to capture a range of conditions and significant variations in the extent of the GHSZ. For Base Case II, to assess the effect of more rapid change, we extrapolate the reported recent 1 ˚C/30 yr trend (Westbrook et al., 2009) to 3 ˚C/100 yr for comparison. In both cases, the total simulation time is restricted, as extrapolation of recent temperature trends over many centuries is speculative at best, and we are most interesting in capturing century-scale phenomena that may already be occurring, and that may already be observable. Base Case II has been examined previously using the same simulation techniques (Reagan and Moridis, 2009) and this work expands upon those simulations and presents a broader range of scenarios.

2.5 Sensitivity

The following variations of the Base Cases, I and II, are also simulated:

Variations in the properties of the hydrate-bearing sediments

Case I.1: Reduced intrinsic permeability

Case I.2: Anisotropy in intrinsic permeability (layered systems)

Case I.3: Importance of horizontal transport

Variations in the thermal properties of the system

Case II.1: Reduced geothermal gradient

Case II.2: Decreased slope angle

Case II.3: Reduced average sediment thermal conductivity

3. RESULTS AND DISCUSSION

While simulating the evolution of the representative hydrate deposit, we record localized methane fluxes through the upper boundary, hydrate dissociation rates, and phase saturations throughout the 2-D system. To simulate such a large system, 80 – 100 processors were required to produce significant results in a manageable amount of time, as the solution of the problem requires the coupled solution of 1.2×10^6 equations at each time step.

3.1 Base Case I: Gradual Change

The base case represents a 3 ˚C temperature change at the seafloor (at all depths from 300 to 550 m) over a 300 yr period. The temperature was varied linearly at a rate of 1 ˚C / 100 yr, with an initial temperature of T_0 = 0 ˚C at t = 0. The upslope limit of the GHSZ at initial conditions is located at x = 290 m, or a water depth of approximately 314 m.

Figure 2 describes the evolution of hydrate saturation, S_H, with time. Minimal change is observed at t = 50 yr, but by t = 100 yr significant recession is apparent (corresponding to the new extent of the GHSZ at time t). At the end of the 300 yr simulation period, the upper (leftmost) extent of methane gas hydrate has receded over 1700 m downslope.

Figure 3 shows the evolution of gas saturation, S_G, with time. At t = 50 yr, only a thin layer of gas is seen along the bottom of the region of hydrate-bearing sediments. By t = 100 yr, a significant region of gas has formed in place of the receding hydrate, with the highest concentration along the bottom of the remaining hydrate and the landward (leftmost) limit of the GHSZ at x = 750 m downslope This gas, now at saturations in excess of the irreducible gas saturation (2%), is moving upward toward the seafloor (z = 0). By t ~ 200 yr, a “plume” of high

gas saturation is observed, reaching the seafloor at x ~ 1400 m. At t = 300 yr, the plume of highest gas saturation is located 2,000 m downslope, and the entire region of the seafloor from x = 500 m to x = 2000 m is receiving mobile methane gas from below.

Note the increase in hydrate saturation ($S_H > S_{H,0}$) in a thin zone along the bottom of the hydrate-bearing sediments for t > 100 yr seen in Figure 2. As gaseous methane (Figure 3) accumulates along the bottom of the remaining hydrate mass (affected by the slightly reduced effective permeability of the overlying hydrate-bearing sediments), secondary hydrate re-forms as some gas enters the (now less extensive) GHSZ. The localized increase in S_H further reduces the effective permeability at the base of the hydrate zone.

Simulation outputs indicate that the first appearance of gaseous methane at the seafloor occurs at about t = 97 yr. In Figure 4, the evolution of gas flux, Q_{CH4}, presented here as mol CH_4 per m^2 at downslope position x for a 1 m-wide 2-D slice of the overall system, is plotted as a function of time, t. The peak of the Q_{CH4} profile corresponds almost exactly to the location of contact between the gas-phase "plume" observed in Figure 3 and the seafloor. The peak Q_{CH4}, as does the plume, moves downslope over time. Localized methane gas flux peaks at 45 mol/yr-m^2 (at t ~ 250 yr) but significant fluxes of gaseous methane occur over a wide area, locally decreasing with time as the subsurface plume moves downslope. This also indicates that the maximum flux, and the lower limit of methane release, aligns with the upper limit of the receding GHSZ.

The evolution of the total methane release at the seafloor, in both aqueous and gaseous form, for the entire 5000 m x 1 m seafloor boundary is shown in Figure 5. Methane release into

the ocean begins just before t = 100 yr, increases continuously over the simulated timeframe, and is still increasing at the end of the simulation at t = 300 yr, having reached 8900 mol/yr.

3.2 Base Case II: Rapid Change

While the Base Case I assumed conservative projections, some observations suggest that warming may in fact be occurring at a considerably faster pace. A change in the temperature of the West Spitsbergen current of 1 ˚C over the past 30 yr has been reported (Westbrook, 2009) with an average rate of 0.03 ˚C /yr. We model such a rapid change with a linear 3 ˚C temperature increase at the seafloor (at all depths from 300 to 550 m) over a 100 yr period with an initial temperature of T_0 = 0 ˚C at t = 0. After 100 years of simulation, the ocean temperature is held constant for additional 100 yr to assess the consequences of the rapid warming. No additional warming is simulated for the reasons stated previously. The simulation is otherwise performed in an identical manner to the base case.

Figure 6 describes the evolution of hydrate saturation, S_H, with time for the case of rapid change. Over the first 200 yr, the upper (leftmost) extent of methane gas hydrate recedes by approximately 1500 m downslope. Moreso than the base case, here we clearly see the effects of the lowering of the top of the GHSZ, as an upper dissociation front is apparent at t = 50 yr, 100 yr, and 130 yr. Simulations of 1-D hydrate-bearing sediment columns under shallow Arctic conditions (Reagan and Moridis, 2008) have demonstrated that the rate of dissociation is regulated by heat transfer limitations, as hydrate dissociation is strongly endothermic, and thus we see the formation of a sharp dissociation front in both the previous 1-D study and in this 2-D simulation. Secondary hydrate formation is less apparent in this case, with only a slight increase in S_H to 0.035 along the bottom of the hydrate-bearing zone at t = 200 yr.

Figure 7 shows the evolution of gas saturation, S_G, with time. At t = 50 yr, a large region of free gas already fills the sediments as the top and bottom of the GHSZ has receded substantially and mobile gas is moving upward toward the seafloor. As in the base case, the gas forms a localized plume of high S_G, which in this case remains well defined as the gas travels through the region between the upper dissociation boundary and the seafloor. This plume contacts the seafloor at x ~ 750 - 1500 m and as in the base case, moves downslope over time, but in this case gas saturations decrease noticeably by t = 130 yr, 30 yr after the end of seafloor temperature changes. By t = 200 yr the entire region of the seafloor from x = 500 m to x = 2200 m is receiving mobile methane gas from below, but S_G within the plume has declined substantially. Simulation outputs indicate that the first appearance of gaseous methane at the seafloor occurs around t ~ 80 yr, and that the onset of gas release is rapid. In Figure 8, the evolution of gas flux, Q_{CH4} (mol/yr-m^2), is presented as a function of time, t, and downslope position, x. The peak of the gaseous flux corresponds closely to the location of the gas-phase plume observed in the 2-D plots of S_G. However, in Base Case II, methane gas flux peaks quickly at 15 mol/yr-m^2 and then slowly decreases with time, and as the hydrate (and the source of methane) recedes downslope.

In contrast to the Base Case I, the distribution of venting is broader, reflecting the greater horizontal extent of high-saturation gas present within the sediment at a given time t. As seen in Figures 3 and 7, the region of free gas extends 750 m further downslope at t = 200 yr when compared to Case I, reflecting more the rapid dissociation of the hydrate.

The evolution of the total methane flux, Q_{CH4}, in both aqueous and gaseous form, for the entire 5000 m x 1 m seafloor boundary is shown in Figure 9. Methane release into the ocean

begins at approximately t = 30 yr in the aqueous phase, but increases rapidly after t = 65 yr until a peak at t = 175 yr at 8800 mol/yr for the 1 m-wide 2-D slice of the overall system. Despite the much more rapid disappearance of hydrate compared to the Case I, the peak flux is nearly identical. Figure 9 also shows the evolution of cumulative release (V_{CH4}) over time, with this Case releasing a total of 9.2×10^5 mol of CH_4 by t = 200 yr. In comparison, at t = 200 yr the base case has released only 3.8×10^5 mol of CH_4. While instantaneous fluxes may be similar for different warming scenarios, more rapid warming clearly results in faster rates of gas release at the seafloor, as would be expected.

3.3 Sensitivity

The simulated cases are schematics, capturing the general behavior of sloping arctic systems, and could be seen as idealized representations of hydrate behavior. The sub-seafloor conditions around the Arctic Ocean margin are liable to vary considerably, however, it is possible to assess a range of possible scenarios to bracket the potential for, and the nature of, methane release due to seafloor temperature changes. Therefore we vary selected geological parameters to estimate the limits of the system.

Case I.1: Reduced intrinsic permeability. The permeability of ocean sediments varies greatly, by up to seven orders of magnitude, depending on sediment type and deposition (Spinelli et al., 2004). Our baseline assumption of $k = 10^{-15}$ m^2 (1 mD) is commonly used for consolidated sediments at the seafloor (Ginsberg and Soloviev, 1998), however, Arctic Ocean terrigenous sediments are likely to have permeabilities ranging from $k = 10^{-13}$ m^2 to $k = 10^{-17}$ m^2 (100 mD to 0.01 mD) (Spinelli et al., 2004). To assess whether the lower values of permeability can mitigate methane release, the Case I "gradual change" scenario (ΔT = 1 ˚C / 100 yr) was re-simulated

using $k = 10^{-16}$ m^2 and $k = 10^{-17}$ m^2. Figure 10 shows the significant consequences of reduced permeability. For $k = 10^{-16}$ m^2 (0.1 mD), instantaneous total flux at the seafloor, Q_{CH4}, is reduced by over 25% over the first 100 yr of simulation. After t = 100 yr, the difference is even more pronounced, lacking the surge in methane flux seen in Base Case I. This is a consequence of a gas-phase release at the seafloor not occurring in the case of reduced-permeability sediments, and methane injection into the water column occurs only through the transport of dissolved methane via the aqueous phase. For $k = 10^{-17}$ m^2 (0.01 mD), Q_{CH4} is reduced by another order of magnitude for the first 100 yr of simulation, although increasing continuously through t = 200 yr. The consequences of this reduced methane release are clear in Figure 11, where the total cumulative methane release, V_{CH4}, is seen to decrease by several orders of magnitude by t = 200 yr due to the permeability reductions.

Case I.2: Anisotropy in intrinsic permeability (layered systems). However, permeability may not be uniform or isotropic. Sedimentary systems are commonly layered, and as such exhibit decreased permeability in the vertical direction, perpendicular to the strata. For Case I.2, the vertical permeability is reduced as in Case I.1, with the horizontal permeability, k_x, remaining at the base value of 10^{-15} m^2 (1 mD). In Figure 10 and Figure 11, the dotted lines present results for anisotropic permeability, and it is clear that vertical permeability, k_z, is the primary factor in flux reduction, as both Q_{CH4} and V_{CH4} for the anisotropic cases are nearly identical to the isotropic reductions used in Case I.1.

Case I.3: Importance of horizontal transport. This observation leads to a further test—for Case I.3, Base Case I was re-simulated without considering any horizontal transport. The horizontal connections were removed entirely from the T+H mesh, shutting down horizontal transport of liquid, gas, or heat. The dotted line in Figures 10 and 11 represents Q_{CH4} and V_{CH4}

for this configuration, and it is clear that vertical transport is responsible for nearly all heat transport into the system and methane flux out of the system. This is not entirely surprising, as the slope of the system is quite shallow, and given the otherwise homogeneous system properties, the 2-D system can be effectively represented by a large number of unconnected 1-D columns.

Case II.1: Reduced geothermal gradient

The geothermal gradient measured at the surface by Haacke et al. (2008) is exceedly high compared to typical global averages, which tend to vary around a mean of about about 3 ˚C / 100 m. Such a steep geothermal gradient results in both a thinner GHSZ as well as more heat available outside the GHSZ (through conduction or fluid advection from below) to fuel the endothermic dissociation reaction. For Case II.1, we reduce the geothermal gradient to 3 ˚C / 100 m, and bring the system back to thermal, chemical, and hydrostatic equilibrium for both a situation where the hydrate extent remains the same as in the Base Cases, and a second sub-case where the extent of hydrate expands to uniformly fill the new, thicker GHSZ. The red and blue lines in Figs. 12 and 13 represent Q_{CH4} and V_{CH4} for the first and second sub-cases, respectively. For both sub-cases, the evolution of the instantaneous flux (Q_{CH4}) and the cumulative flux (V_{CH4}) is remarkably similar, with both sub-cases exhibiting a 54% decrease in instantaneous flux by t = 200 yr and a corresponding 71% decrease in the cumulative methane released over the simulated seafloor boundary as a result of the shallower gradient. The arrival of gaseous methane at the seafloor is delayed by 40 yr for both sub-cases. Somewhat surprising is that the increasing the mass of hydrate has little effect on the flux, at least in the short term, suggesting again that the driving force that moves gaseous methane toward the seafloor is buoyancy, and simply increasing the extent of the zone of hydrate-derived free gas from dissociation does not increase the flux (although a larger extent of hydrate would also mean a greater total quantity of gas once

dissociation is complete, and perhaps a longer period of methane flux, but this is not a factor at short time scales).

Case II.2: Decreased slope angle. Slope angles vary considerably throughout the regions where methane flares or plumes have been observed. However, any sloping system will still be subject to a variation of seafloor pressure with depth, and hence rising temperatures will move the top of the GHSZ downslope. To assess the rate of recession as a function of slope steepness, we next reduced the slope angle of the system in Case II.1 (the case of a reduced geothermal gradient with increased hydrate extent) to 3.5%, with the upper $x = 0$ boundary remaining at a depth of 300 m, and then re-equilibrate the system to adjust the location of the GHSZ in the sediments (and removing hydrate now outside the new GHSZ). The system is brought to thermal, chemical, and hydrostatic equilibrium, then the Case II warming scenario (3 ˚C/100 yr) was applied. The resulting fluxes (Figure 12) are notably larger than for Case II.1, and cumulative release (Figure 13) is up to 100% greater by $t = 200$ yr. This is a consequence of the shallow slope exposing a greater region of the GHSZ to destabilization (due to lower pressures from relatively shallower depths vs. x) at a given time t, and the corresponding higher dissociation rate driving greater methane release through the seafloor boundary.

Case II.3: Reduced average sediment wet thermal conductivity. Laboratory studies of thermals properties of hydrate-bearing sediments, coupled with inverse modeling (Moridis et al., 2005), lead to estimates of wet sediment thermal conductivity, k_{Sw}, of about 3.1 W/mK for hydrate-bearing media. However, marginal sediments, such as those observed offshore in deeper locations further offshore (Haake et al., 2008; Jansen and Raymo, 1996) may exhibit lower thermal conductivities, although not necessarily in the presence of hydrates. As Case II.1 reduced heat flow through the system by reduction in the geothermal gradient, this Case reduces heat

flow by a factor of three through the lowering of the k_{Sw} to 1.0 W/mK from the Base Case II value of k_{Sw} = 3.1 W/mK. The system is again brought to thermal, chemical, and hydrostatic equilibrium at the new sediment properties, while all other properties and simulation parameters (including the geothermal gradient and slope angle) remain the same as in Base Case II. The resulting fluxes (Figure 12) indicate a delay of about 15 yr for the appearance of released gas at the seafloor, with fluxes reduced by 66% at t = 100 yr and by only 20% by t = 200 yr. Cumulative fluxes (Figure 13) for Case II.3 are reduced 37% by t = 200 yr. Although the ability of the system to transfer heat from either the warming seafloor sediments above the deposit or from deeper, warmer sediments is reduced, dissociation and the release of gas is only somewhat mitigated.

4. CONCLUSIONS

4.1 Comparison to 1-D results

Previous simulations of 1-D hydrate-bearing sediment columns (Reagan and Moridis, 2008) indicated that hydrate dissociation due to both gradual and rapid change does not produce violent eruptions of methane gas, rather, dissociation and the resultant gas release tend to occur in an orderly fashion, regulated by heat transfer limitations and gas migration through sediments containing multiple phases. Extending the model system to a 2-D sloping domain introduces horizontal migration of fluids and dissociation of hydrate along multiple fronts. However, the rate of dissociation and the rate of gas release into the environment are still constrained by heat and fluid flow limitations, and as such these deposits release gas at the seafloor in an orderly fashion. In both the Base Case and Case II in particular, we see the formation of a sharp upper dissociation boundary and instantaneous total methane fluxes that asymptotically approach a

constant value, similar to the example of a 1-D Arctic hydrate system at T = 0.4 ˚C and 320 m depth (Reagan and Moridis, 2008). Substantial but not catastrophic releases appear to be the likely consequence of climate-driven hydrate dissociation on this scale, unless additional overpressured free gas (not simulated here) underlies a geomechanically susceptible overburden supported by the hydrates. Coupled flow-geomechanical simulations of sloping hydrate-bearing systems may be necessary to further characterize such systems.

4.2 Comparison to Observations

A team led by Westbrook (Westbrook et al., 2009) recently observed over 250 plumes of methane gas erupting from the seabed off the West Spitsbergen (Svalbard) continental margin at the present landward limit of the GHSZ (near 400 m water depth). These gas plumes, which extend along 30 km of the slope, have been hypothesized to be partly the result of hydrate dissociation as a consequence of recent ocean warming in the area, and partly due to diversion and channeling of upwelling methane by hydrate-bearing sediments. Using hydrate saturations taken (about 4.5% average) from further downslope, the observers estimated a potential release of 900 kg/yr CH_4 per 1 m of margin length.

The simulations presented in this paper closely represent the type and extent of hydrate-bearing system thought to exist along the Svalbard margin, and allow us to make several conclusions about the nature of such a system:

(1) Our simulations, using a slightly lower average $S_{H,0}$, suggest that 141 kg/yr CH_4 per 1 m width of slope can be released solely due to dissociating hydrate. Integrated over the 30 km plume region, this would be 0.004 Tg/yr of CH_4 from this one hydrate system alone, small in

comparison to the global atmospheric flux of methane but significant to the ocean biochemistry of the region. Our simulations also indicate that shallow hydrate systems are sensitive to ocean warming on decadal timescales, and that the methane release could occur after less than a century of warming. Recent simulations of methane release into a biologically active ocean model (Elliott et al., 2011) suggest that hydrate systems generating fluxes of this magnitude over a wider area (for example, if such release occurs along a longer stretch of Arctic Ocean continental shelf) could release enough methane to create significant biochemical changes in the water column, whether or not the methane reaches the atmosphere.

(2) A second conclusion from this study is that hydrate alone can provide a significant quantity of methane gas in climate change-driven release scenarios, in addition to any geological methane source that may be providing free gas or dissolved aqueous methane to the region below the GHSZ. Assessing the total potential contribution of such shallow hydrate systems is currently an active area of research. While systems with free gas capped by hydrates may indeed lead to the formation of methane plumes (perhaps via eruption after the removal of the hydrate cap), it is clear that sparse hydrates alone can contribute significantly to the total release.

(3) A third conclusion is that sloping, shallow hydrate-bearing systems release methane as localized “plumes” of higher flux, despite the very low hydrate saturations expected for disperse, unconfined stratigraphic deposits and despite the relative unimportance of horizontal transport along the bottom of the GHSZ. For systems with substantial gas saturations, we see no significant horizontal diversion of gas flow due to the reduced effective permeability of hydrate-bearing sediments, the trapping of methane through the formation of secondary hydrate when methane enters the GHSZ, and the increased effective permeability of an extensive free-gas zone. Such a diversion of gas flow is not required to form localized subsurface plumes of higher

methane saturation. Dissociation of hydrate and the upward transport of gas via buoyancy provides a model for the formation of gas plumes at the landward limit of the GHSZ, as has been observed. A free-gas zone underneath such a hydrate deposit is likely to contribute to the resultant methane fluxes in the scenarios represented here, but is not likely to be the primary source of gas flux in the shorter term, as even sparse hydrate contains more methane per unit volume that what is found in typical methane-bubble regions below the BSR.

4.3 Sensitivity Analysis

The properties of sloping systems along continental margins are likely to vary considerably from location to location, and a sensitivity analysis of the two temperature-change scenarios suggests which properties are mostly likely to impact system behavior.

(1) For Case I, reduction in vertical sediment intrinsic permeability has profound effects on methane release at the seafloor, with permeabilities of order $k = 10^{-15}$ m^2 (1 mD) required to achieve significant gas fluxes. This model does not include high-permeability pathways, such as fractures, faults, conduits, or channels, and as such should represent conservative release estimates. Horizontal permeability is not a factor for this system configuration, with neither anisotropy (increased horizontal permeability, Case I.2) nor the mere presence of any horizontal permeability whatsoever (Case I.3) altering the magnitude of methane flux. This seems surprising, given the typical conceptualization of the hydrate layer as a “cap” or barrier that diverts fluid flow (Westbrook et al., 2009), but in this case, the change in effective permeability due to the sparse hydrate is minimal, and the existence of the GHSZ as a barrier (through the capture of gas as solid hydrate) is minimized due to the warming of the sediments, the recession of the GHSZ, and the rapid dissociation of the hydrate, on timescales faster than that at which the

gas rises upward. A more saturated hydrate layer would be required to form a low-permeability barrier. This suggests that for sparse, shallow hydrates, a 1-D model of the system may indeed be effective for modeling bulk dissociation of hydrate due to ocean warming (Reagan and Moridis, 2008). Such a 1-D model greatly simplifies the simulation-based assessment of wider regions (i.e. basin-scale) and assists in the potential coupling of sediment/subseafloor models to ocean and climate simulators.

(2) In the sensitivity study of Case II, it is interesting that none of the studied effects, geothermal gradient steepness (with or without extended GHSZ), slope angle changes, or sharp reductions in the intrinsic thermal conductivity of wet sediments, resulted in a complete mitigation of gas release at the seafloor.

ACKNOWLEDGMENTS

This research was funded by the Assistant Secretary for Fossil Energy, Office of Natural Gas and Petroleum Technology, through the National Energy Technology Laboratory, and by the Director, Office of Science, Office of Biological and Environmental Research of the U.S. Department of Energy, under Contract No. DE-AC02-05CH11231. The authors would like to thank Katie L. Boyle for the development of the 2-D data visualization tools, Keni Zhang for development of the parallel TOUGH+HYDRATE code, and Heidi A. Kuzma for insightful pre-review.

REFERENCES

Archer, D., Buffett, B., and V. Brovkin, Ocean methane hydrates as a slow tipping point in the global carbon cycle. *PNAS*, 106(49), 20596-20601, 2009.

Borowski, W.S., A review of methane and gas hydrates in the dynamic, stratified system of the Blake Ridge region, offshore southeastern North *America. Chem. Geology*, 205, 311-346, 2004.

Buffett, B., and D. Archer, Global inventory of methane clathrate: Sensitivity to changes in environmental conditions, *Earth Planetary Sci. Lett*., 227, 185-199, 2004.

Elliott, S.M., Maltrud, M., Reagan, M.T., Moridis, G.J., Cameron-Smith, P.J.: Marine Methane Cycle Simulations for the Period of Early Global Warming, *J. Geophysical Res. Biogeo.*, 116, G01010, 2011.

GEBCO, Published by the British Oceanographic Data Centre on behalf of Intergovernmental Oceanographic Commission and International Hydrographic Organization, 1997.

Ginsburg, G.D. and V.A. Soloviev, *Submarine Gas Hydrates*. St. Petersburg, 1998.

Gornitz V., and I. Fung, Potential distribution of methane hydrate in the world's oceans, *Global Biogeochem. Cycles*, 8, 335-347, 1994.

Haake, R.R., Westbrook, G.K., and M.S. Riley, Controls on the formation and stability of gas hydrate-related bottom-simulating reflectors (BSRs): A case study from the west Svalbard continental slope, *J. Geophys. Res.*, 113, B05104, doi: 10.1029/2007JB005200, 2008.

Hovland, M., Svensen, H., Forsberg, C.F., Johansen, H., Fichler, C., Fossa, J.H., Jonsson, R., and H. Rueslatten, Complex pockmarks with carbonate-ridges off mid-Norway: Products of sediment degassing, *Marine Geology*, 218, 191-206, 2005.

Jansen, E., Raymo, M.E., Blum, P., et al., *Proc. ODP, Initial Reports,* 162, 287-343, 1996.

Kennett, J.P., Cannariato, K.G., Hendy, L.L., and R.J. Behl, Carbon isotopic evidence for methane hydrate instability during quaternary interstadials. *Science*, 288, 128-133, 2000.

Kennett, J.P., Cannariato, K.G., Hendy, L.L., and R.J. Behl, *Methane hydrates in quaternary climate change: The Clathrate Gun Hypothesis*, AGU Publishing, Washington, DC, 2002.

Klauda, J.B., and S.I. Sandler, Global distribution of methane hydrate in ocean sediment. *Energy and Fuels*, 19, 459-470, 2005.

Kvenvolden, K.A., Potential effects of gas hydrate on human welfare, *Proc. Nat. Acad. Sci*., *96*, 3420-3426, 1999.

Mascarelli, A.L., A Sleeping Giant? *Nature Reports Climate Change*, 3, 4, doi: 10.1038/ climate.2009.24, 2009.

Meehl, G., et al., Global climate projections, *Climate Change 2007: The Physical Basis*, pp. 789-844, Cambridge Univ. Press, Cambridge, UK, 2007.

Moridis, G.J., Numerical Studies of Gas Production from Methane Hydrates, *SPE Journal*, 32, 8, 2003.

Moridis, G.J., Seol, Y., and T. Kneafsey, Studies of reaction kinetics of methane hydrate dissociation in porous media (Paper 1004), *Proceedings of the 5th International Conference on Gas Hydrates*, Trondheim, Norway, 12-16 June 2005.

Moridis, G.J., and M.B. Kowalsky, Response of Oceanic Hydrate-Bearing Sediments to Thermal Stresses, *SPE Journal*, *12*(2), 253-268, doi:10.2118/111572-PA, 2007.

Moridis, G.J., Kowalsky, M.B., and K. Pruess, *TOUGH+HYDRATE v1.0 User's Manual: A Code for the Simulation of System Behavior in Hydrate-Bearing Geologic Media,* Report LBNL-0149E, Lawrence Berkeley National Laboratory, Berkeley, CA.

Reagan, M. T., and G. J. Moridis, Dynamic response of oceanic hydrate deposits to ocean temperature change, *J. Geophys. Res*., 113, C12023, doi:10.1029/2008JC004938, 2008.

Reagan, M. T., and G. J. Moridis, Large-Scale Simulation of Methane Hydrate Dissociation along the West Spitsbergen Margin, *Geophys. Res. Lett.*, 36, L23612, doi:10.1029/2009GL041332, 2009.

Sloan, E.D. and C. Koh, *Clathrate Hydrates of Natural Gases*, CRC Press, New York, NY, 2008.

Spinelli, G.A., Giambalvo, E.R., and Fisher, A.T., *Sediment permeability, distribution, and influence on fluxes in oceanic basement.* Hydrogeology of the Oceanic Lithosphere, E.E. Davis and H Elderfield, Eds. Cambridge University Press, 2004.

Stone, H.L., Probability model for estimating three-phase relative permeability, *Trans. SPE AIME*, 249, 214-218, 1970.

Westbrook, G.K., Thatcher, K.E, Rohling, E.J., Piotrowski, A.M., Palike, H., Osborne, A.H., Nisbet, E.G., Minshull, T.A., Lanoiselle, M., James, R.H., Huhnerbach, V., Green, D., Fisher, R.E., Crocker, A.J., Chabert, A., Bolton, C., Beszczynska-Moller, A., Berndt, C., and A. Aquilina, Escape of methane gas from the seabed along the West Spitsbergen continental margin *Geophys. Res. Lett.*, 36, L15608, doi: 10.1029/2009GL039191, 2009.

Van Genuchten, M.T., A closed-form equation for predicting the hydraulic conductivity of unsaturated soils, *Soil Sci. Soc*., 44, 892-898, 1980.

LIST OF CAPTIONS

Figure 1. Illustration of the domain discretization, GHSZ extent, and boundaries for for the 2-D sloping system, representing a 5 km slice of the Arctic continental shelf (not to scale). Gridlines are a schematic representation only.

Figure 2. Hydrate saturation, S_H, for the 2-D system at t = 50, 100, 200, and 300 yr for Base Case I, a 3˚C temperature increase at the seafloor over 300 yr. The top of the 5% slope is at x = 0. Note the recession of the hydrate downslope due to temperature-driven dissociation.

Figure 3. Gas saturation, S_G, for the 2-D system at t = 50, 100, 200, and 300 yr for Base Case I, a 3˚C temperature increase at the seafloor over 300 yr. The top of the 5% slope is at x = 0.

Figure 4. Flux of gaseous methane, Q_{CH4}, at the seafloor at at t = 100, 150, 200, 250, and 300 yr. Q_{CH4} is presented here as mol CH_4 per m^2 at downslope position x for a 1 m-wide 2-D slice of the real system, for Base Case I. Note that the location of the maximum flux moves downslope as warming progresses, and that this maximum is aligned with the upper limit of the GHSZ at a given time.

Figure 5. Total methane release (aqueous and gaseous phases), $Q_{CH4,T}$ (red line), and cumulative methane release, V_{CH4}, (blue line) for the entire simulated seafloor boundary, a 1 m-wide, 5000 m long section, for Base Case I.

Figure 6. Hydrate saturation, S_H, for the 2-D system at t = 50, 100, 130, and 200 yr for Base Case II, a 3˚C temperature increase at the seafloor over 100 yr followed by 100 yr of constant T. The top of the 5% slope is at x = 0. Note the establishment of an upper dissociation front at t = 50, 100, and 130 yr.

Figure 7. Gas saturation, S_G, for the 2-D system at t = 50, 100, 130, and 200 yr for Base Case II, a 3˚C temperature increase at the seafloor over 100 yr followed by 100 yr of constant T. The top of the 5% slope is at x = 0. Note the localized zone of high gas saturation (S_G > 0.18) that extends from the upper dissociation front to the seafloor.

Figure 8. Flux of gaseous methane, Q_{CH4}, at the seafloor at t = 85, 100, 130, 160, and 200 yr for Base Case II. Q_{CH4} is presented here as mol CH_4 per m^2 at downslope position x for a 1 m-wide 2-D slice of the real system. Note that the location of the maximum flux moves downslope as warming progresses, and that this maximum is aligned with the upper limit of the GHSZ at a given time.

Figure 9. Total methane release (aqueous and gaseous phases), $Q_{CH4,T}$ (red line), and cumulative methane release, V_{CH4} (blue line) over the entire simulated seafloor boundary, a 1 m-wide, 5000 m long section, for Base Case II.

Figure 10. Variation of total methane release (aqueous and gaseous phases), $Q_{CH4,T}$ as a function of (Case I.1) permeability, (Case I.2) anisotropy, and (Case I.3) limited horizontal transport for Case I over the entire simulated seafloor boundary, a 1 m-wide, 5000 m long section.

Figure 11. Variation of cumulative methane release (aqueous and gaseous phases), $V_{CH4,T}$ as a function of (Case I.1) permeability, (Case I.2) anisotropy, and (Case I.3) horizontal transport for Case I over the entire simulated seafloor boundary, a 1 m-wide, 5000 m long section.

Figure 12. Variation of total methane release (aqueous and gaseous phases), $Q_{CH4,T}$ as a function of (II.1) decreased geothermal gradient, (II.1) the resulting change in GHSZ extent, (II.2) slope angle, and (II.3) sediment thermal conductivity for Case II over the entire simulated seafloor boundary, a 1 m-wide, 5000 m long section.

Figure 13. Variation of cumulative methane release (aqueous and gaseous phases), $V_{CH4,T}$ as a function of (II.1) decreased geothermal gradient, (II.1) the resulting change in GHSZ extent, (II.2) slope angle, and (II.3) sediment thermal conductivity for Case II over the entire simulated seafloor boundary, a 1 m-wide, 5000 m long section.

Table 1. Physical properties and simulation parameters for the 2-D hydrate-bearing system.

Parameter	Value
Initial pore water salt mass fraction, X_0	0.035
Permeability, k	10^{-15} - 10^{-17} (= 1 mD – 0.01 mD)
Porosity, ϕ (Haake et al., 2008)	0.55
Dry thermal conductivity, k_{Sd}	1.0 W/m/K
Wet thermal conductivity, k_{Sw} (Moridis et al, 2005)	3.3 W/m/K
Composite thermal conductivity k_Θ model (Moridis et al., 2005)	$k_\Theta = (\sqrt{S_H} + \sqrt{S_A}) * (k_{Sw} - k_{Sd}) + k_{Sd}$
Capillary pressure model (van Genuchten, 1980)	$P_{cap} = -P_0 \left[(S^*)^{-1/\lambda} - 1 \right]^{\lambda}$ $S^* = \frac{(S_A - S_{irA})}{(S_{mxA} - S_{irA})}$
P_0	2000 Pa
Relative permeability model (Stone, 1970)	$k_{rA} = (S_A^*)^n$ $k_{rG} = (S_G^*)^n$ $S_A^* = (S_A - S_{irA})/(1 - S_{irA})$ $S_G^* = (S_G - S_{irG})/(1 - S_{irA})$
λ	0.45
n	4
S_{irG}	0.02
S_{irA}	0.20

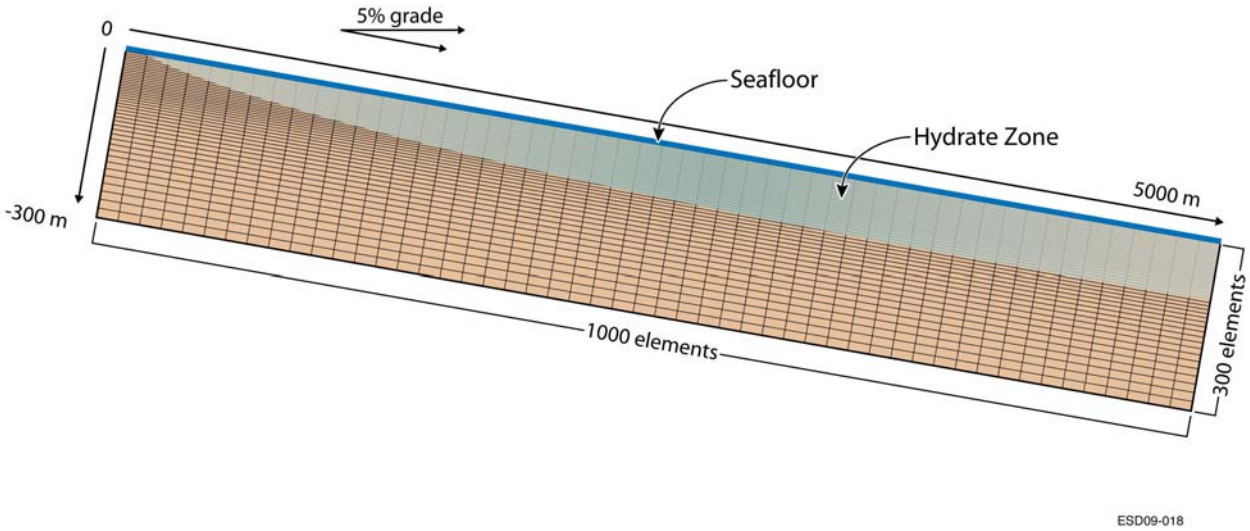

Figure 1. Illustration of the domain discretization, GHSZ extent, and boundaries for for the 2-D sloping system, representing a 5 km slice of the Arctic continental shelf (not to scale). Gridlines are a schematic representation only.

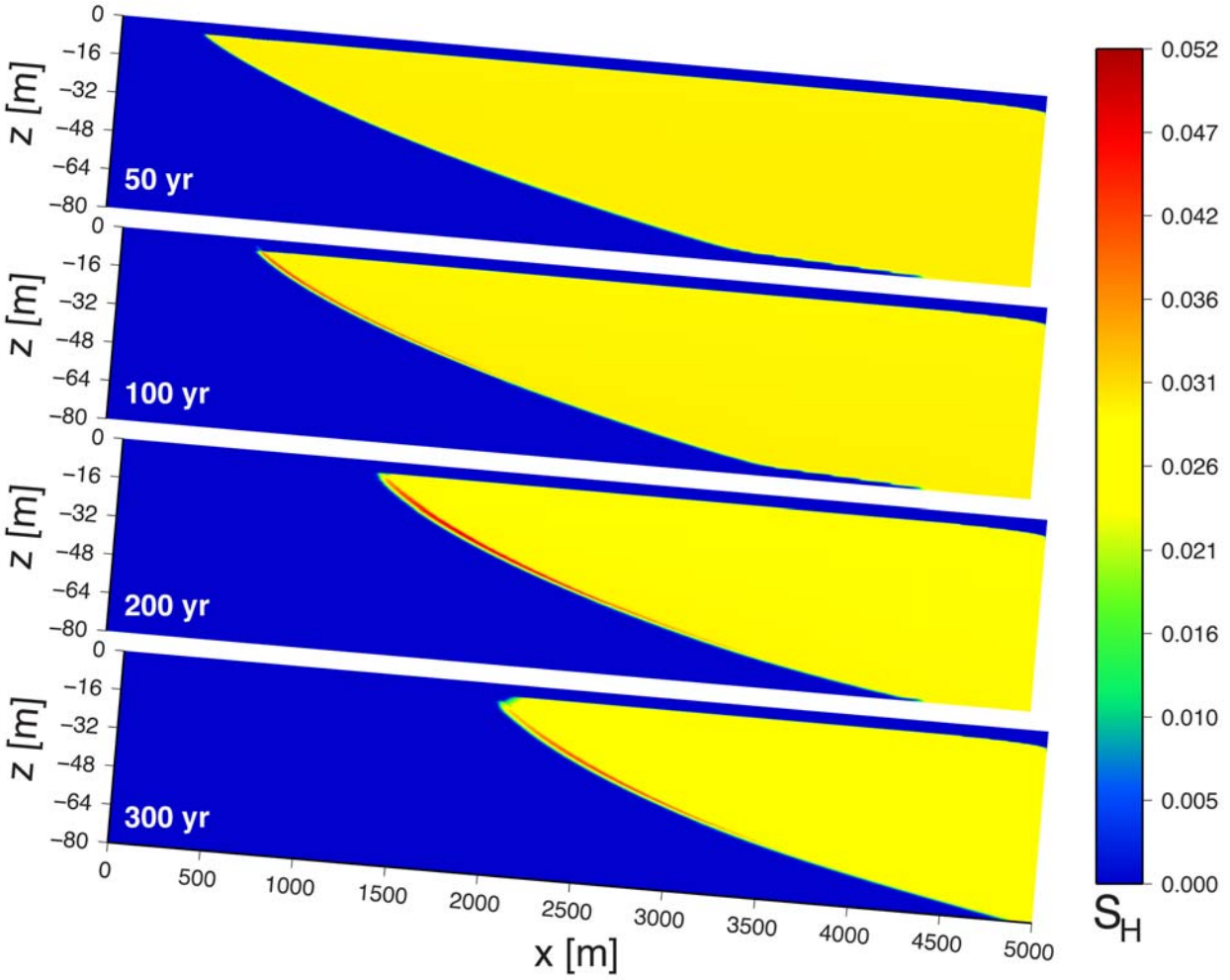

Figure 2. Hydrate saturation, S_H, for the 2-D system at t = 50, 100, 200, and 300 yr for Base Case I, a 3˚C temperature increase at the seafloor over 300 yr. The top of the 5% slope is at x = 0. Note the recession of the hydrate downslope due to temperature-driven dissociation.

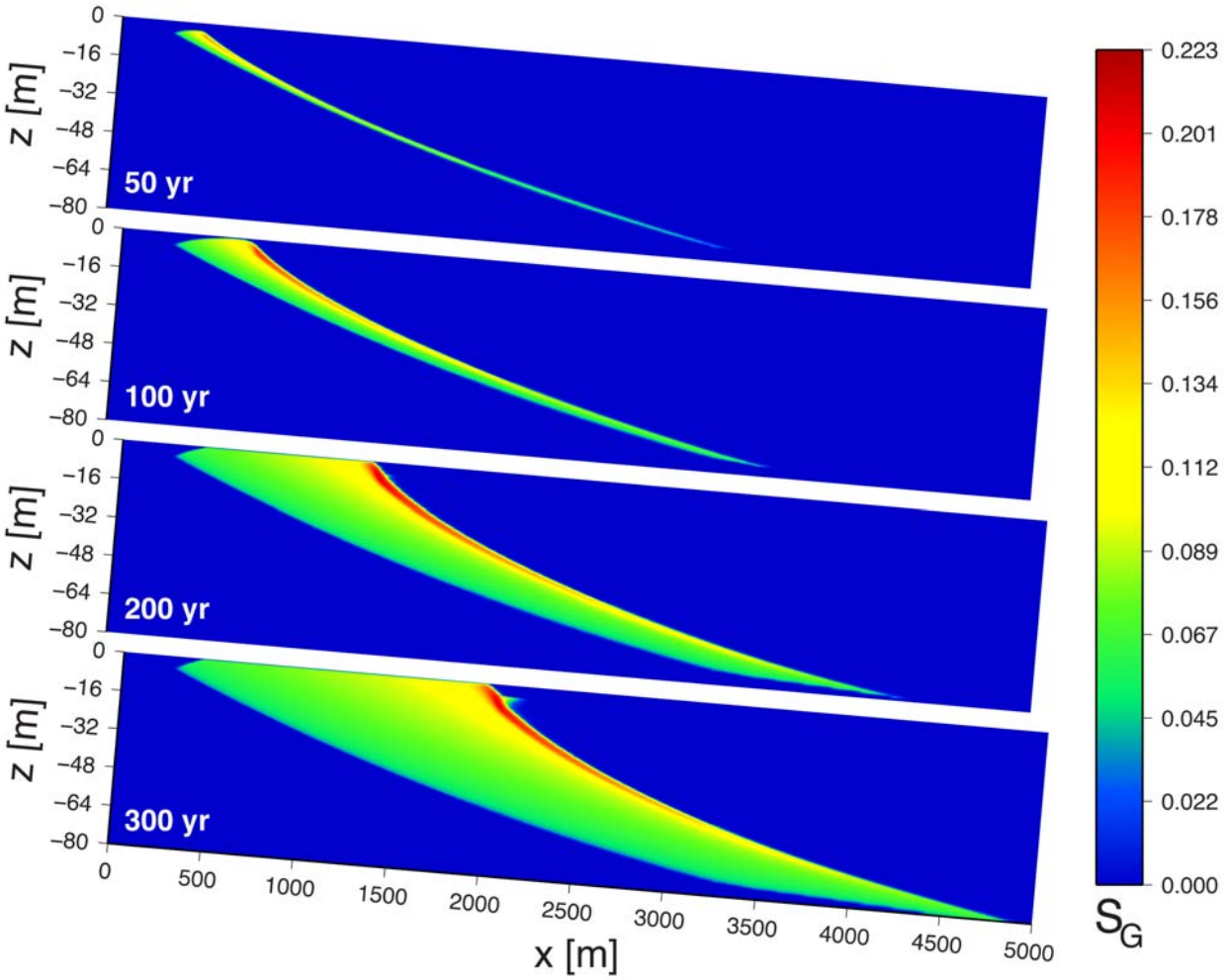

Figure 3. Gas saturation, S_G, for the 2-D system at t = 50, 100, 200, and 300 yr for Base Case I, a 3˚C temperature increase at the seafloor over 300 yr. The top of the 5% slope is at x = 0.

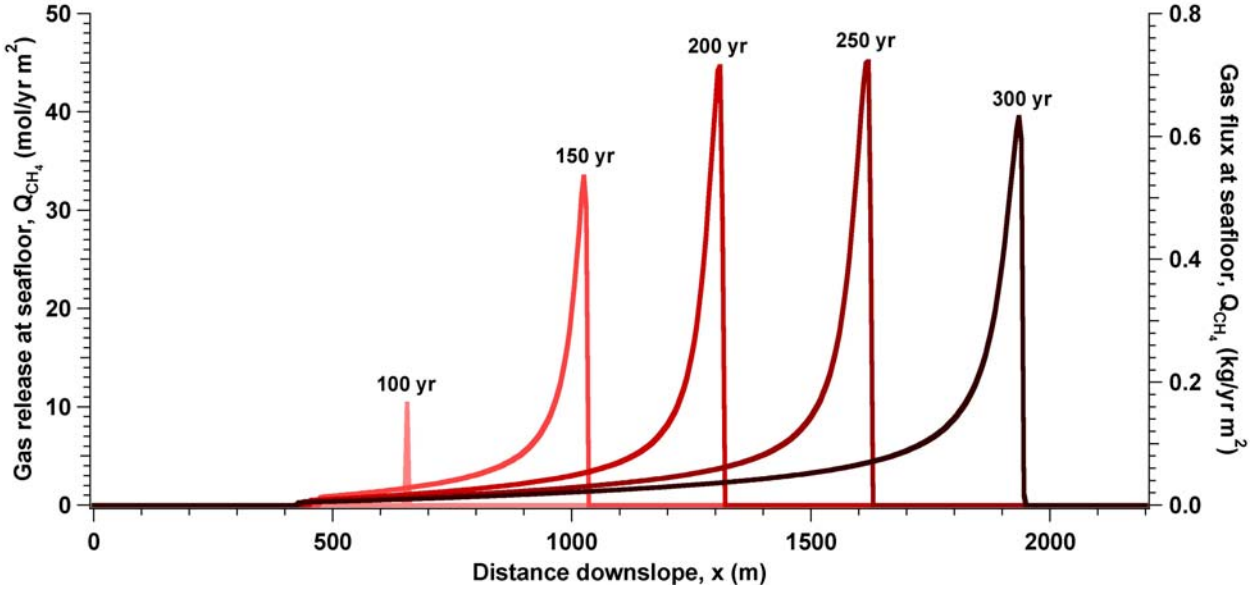

Figure 4. Flux of gaseous methane, Q_{CH4}, at the seafloor at at t = 100, 150, 200, 250, and 300 yr. Q_{CH4} is presented here as mol CH_4 per m^2 at downslope position x for a 1 m-wide 2-D slice of the real system, for Base Case I. Note that the location of the maximum flux moves downslope as warming progresses, and that this maximum is aligned with the upper limit of the GHSZ at a given time.

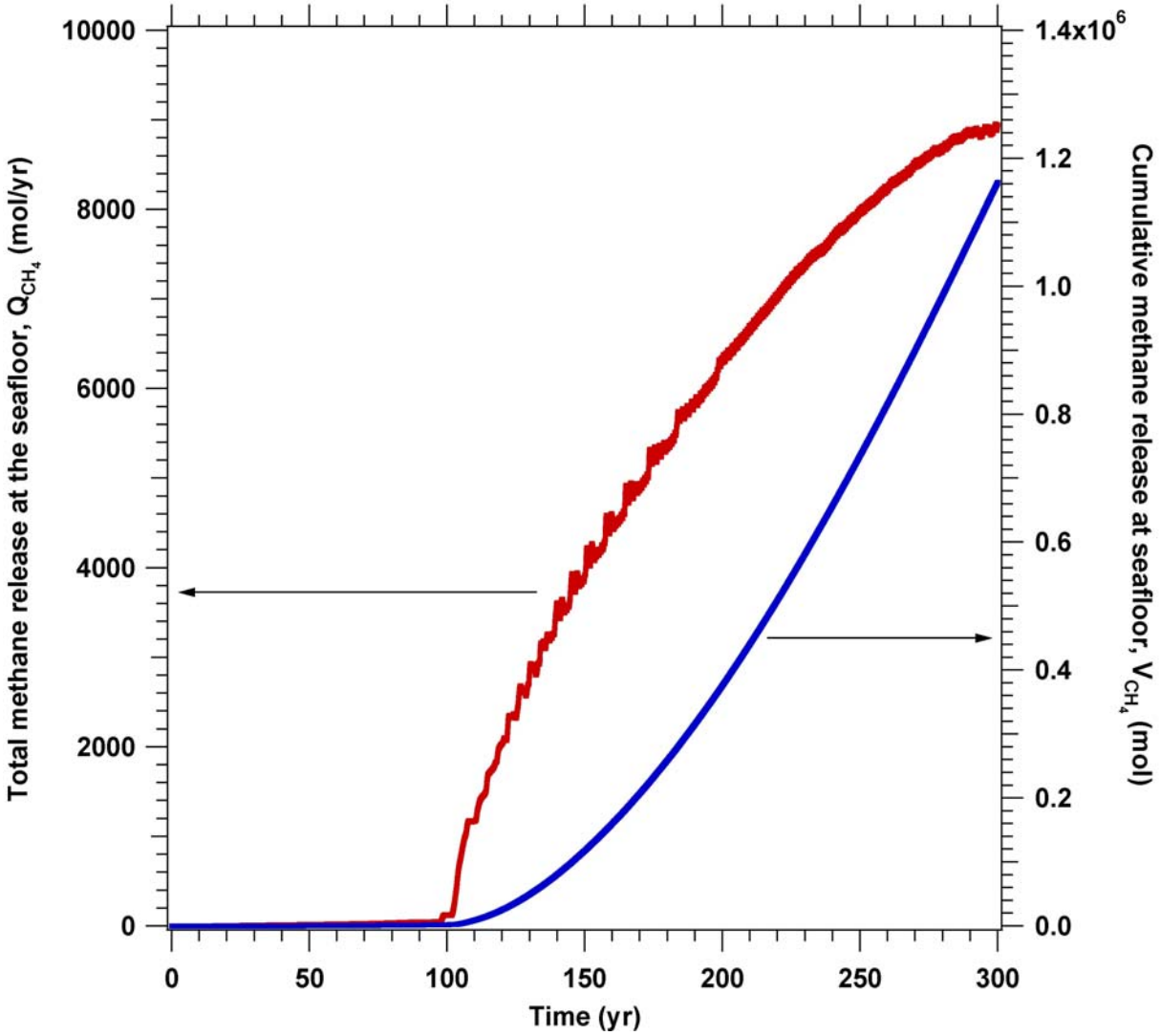

Figure 5. Total methane release (aqueous and gaseous phases), $Q_{CH4,T}$ (red line), and cumulative methane release, V_{CH4}, (blue line) for the entire simulated seafloor boundary, a 1 m-wide, 5000 m long section, for Base Case I.

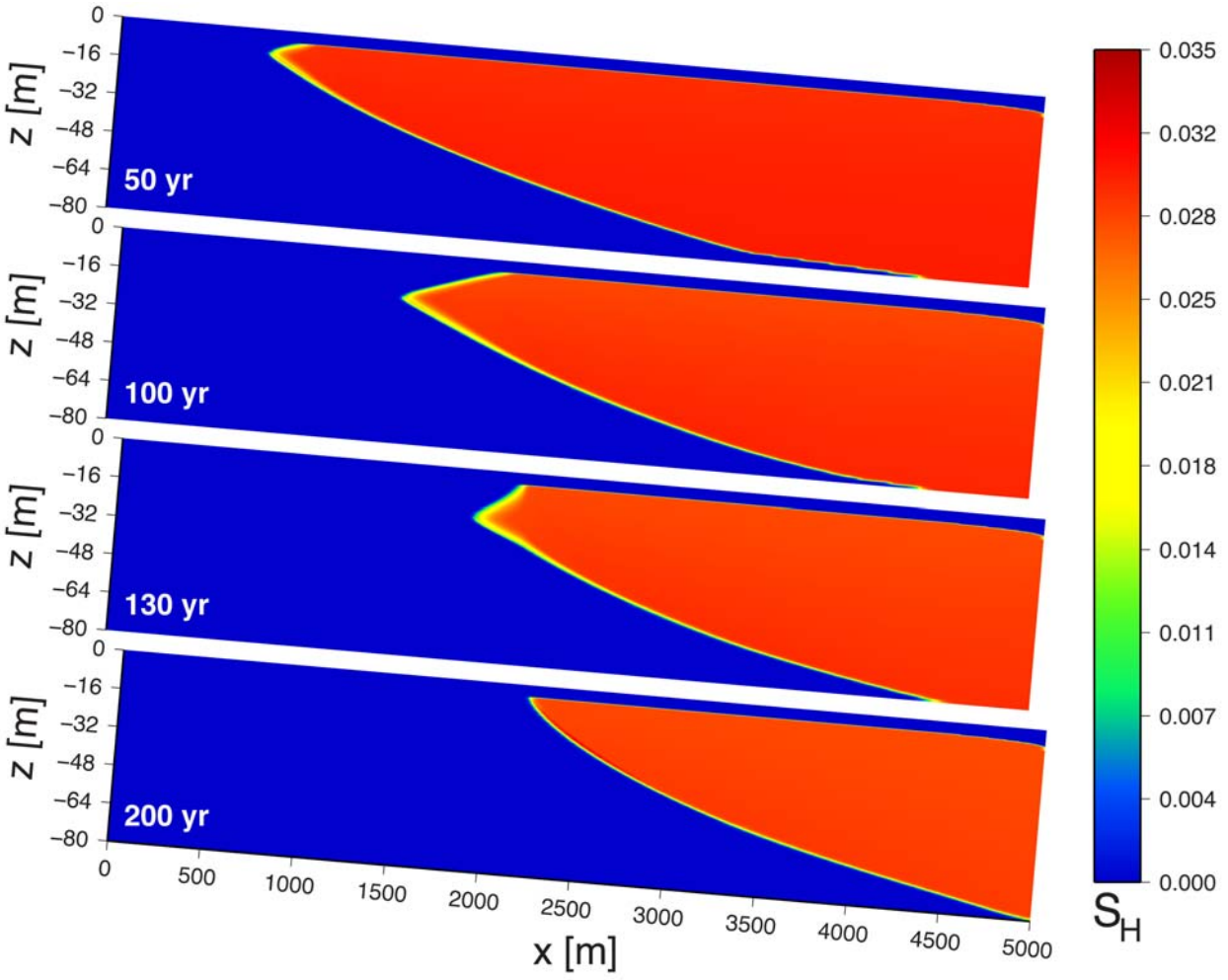

Figure 6. Hydrate saturation, S_H, for the 2-D system at t = 50, 100, 130, and 200 yr for Base Case II, a 3˚C temperature increase at the seafloor over 100 yr followed by 100 yr of constant T. The top of the 5% slope is at x = 0. Note the establishment of an upper dissociation front at t = 50, 100, and 130 yr.

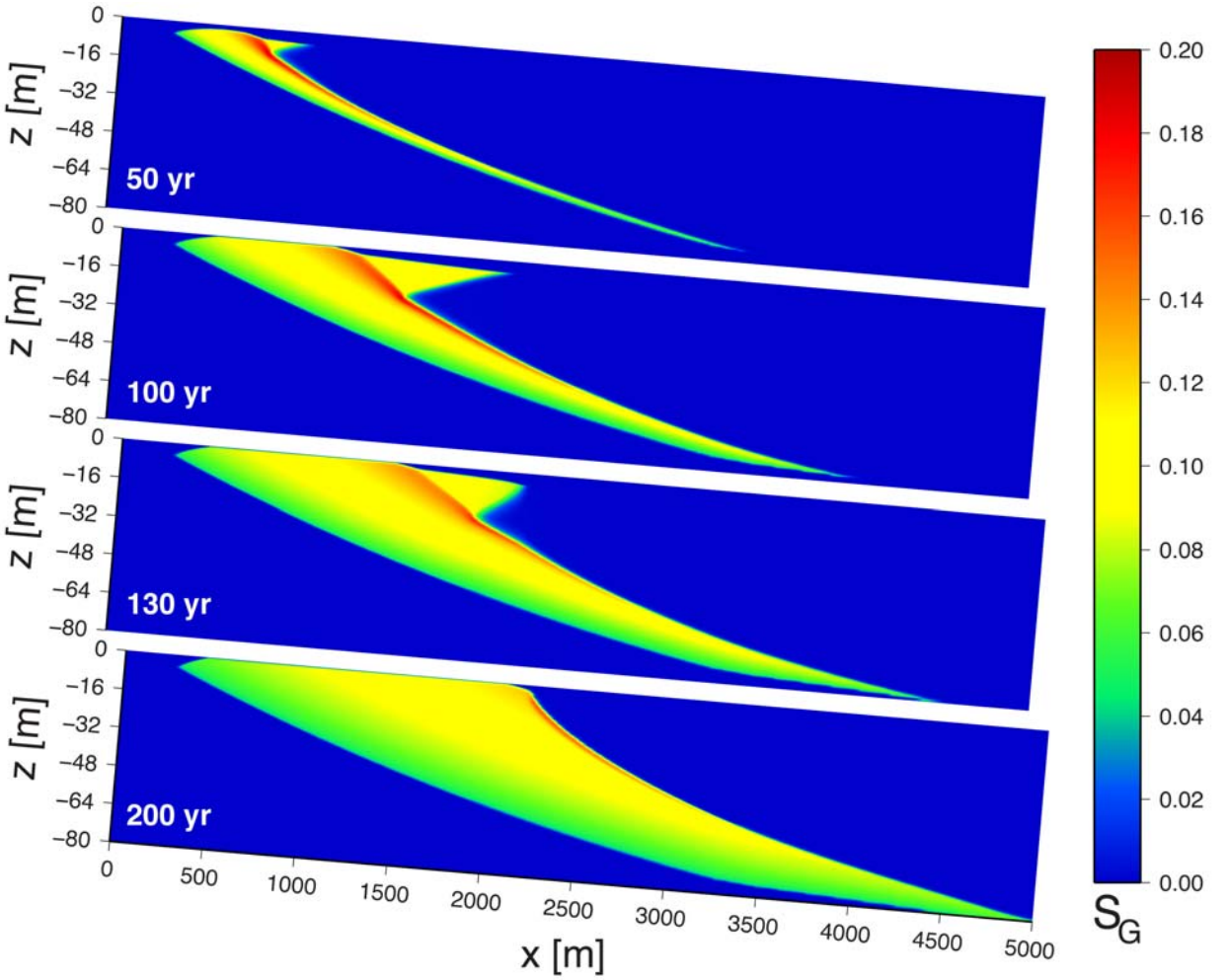

Figure 7. Gas saturation, S_G, for the 2-D system at t = 50, 100, 130, and 200 yr for Base Case II, a 3˚C temperature increase at the seafloor over 100 yr followed by 100 yr of constant T. The top of the 5% slope is at x = 0. Note the localized zone of high gas saturation (S_G > 0.18) that extends from the upper dissociation front to the seafloor.

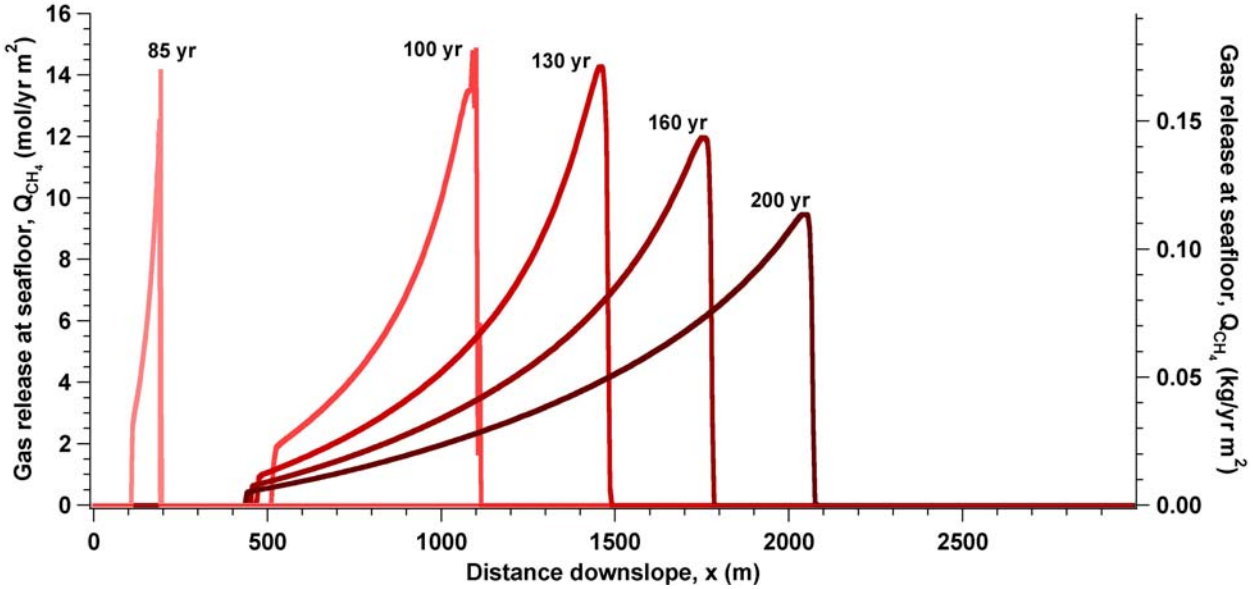

Figure 8. Flux of gaseous methane, Q_{CH4}, at the seafloor at t = 85, 100, 130, 160, and 200 yr for Base Case II. Q_{CH4} is presented here as mol CH_4 per m^2 at downslope position x for a 1 m-wide 2-D slice of the real system. Note that the location of the maximum flux moves downslope as warming progresses, and that this maximum is aligned with the upper limit of the GHSZ at a given time.

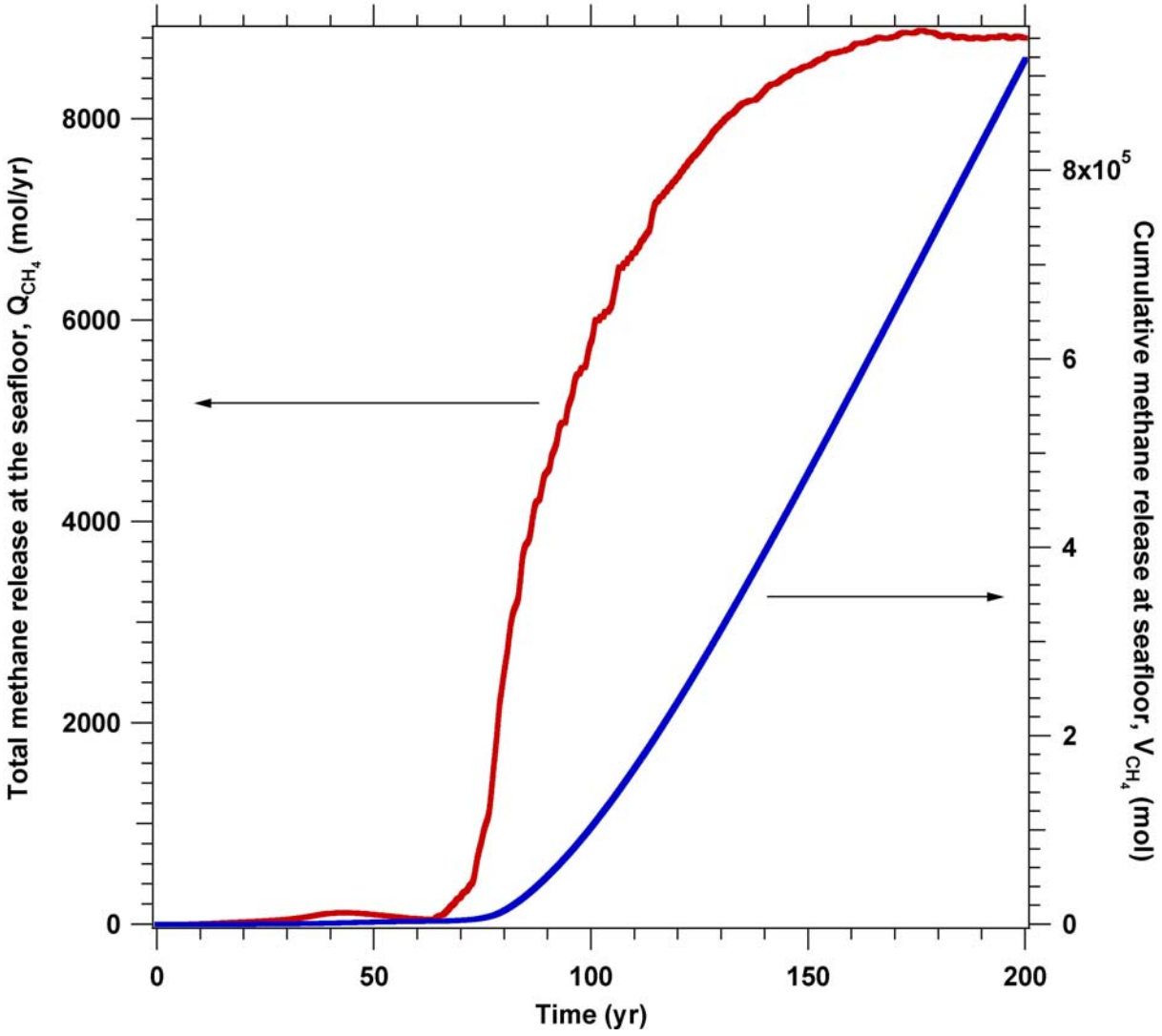

Figure 9. Total methane release (aqueous and gaseous phases), $Q_{CH4,T}$ (red line), and cumulative methane release, V_{CH4} (blue line) over the entire simulated seafloor boundary, a 1 m-wide, 5000 m long section, for Base Case II.

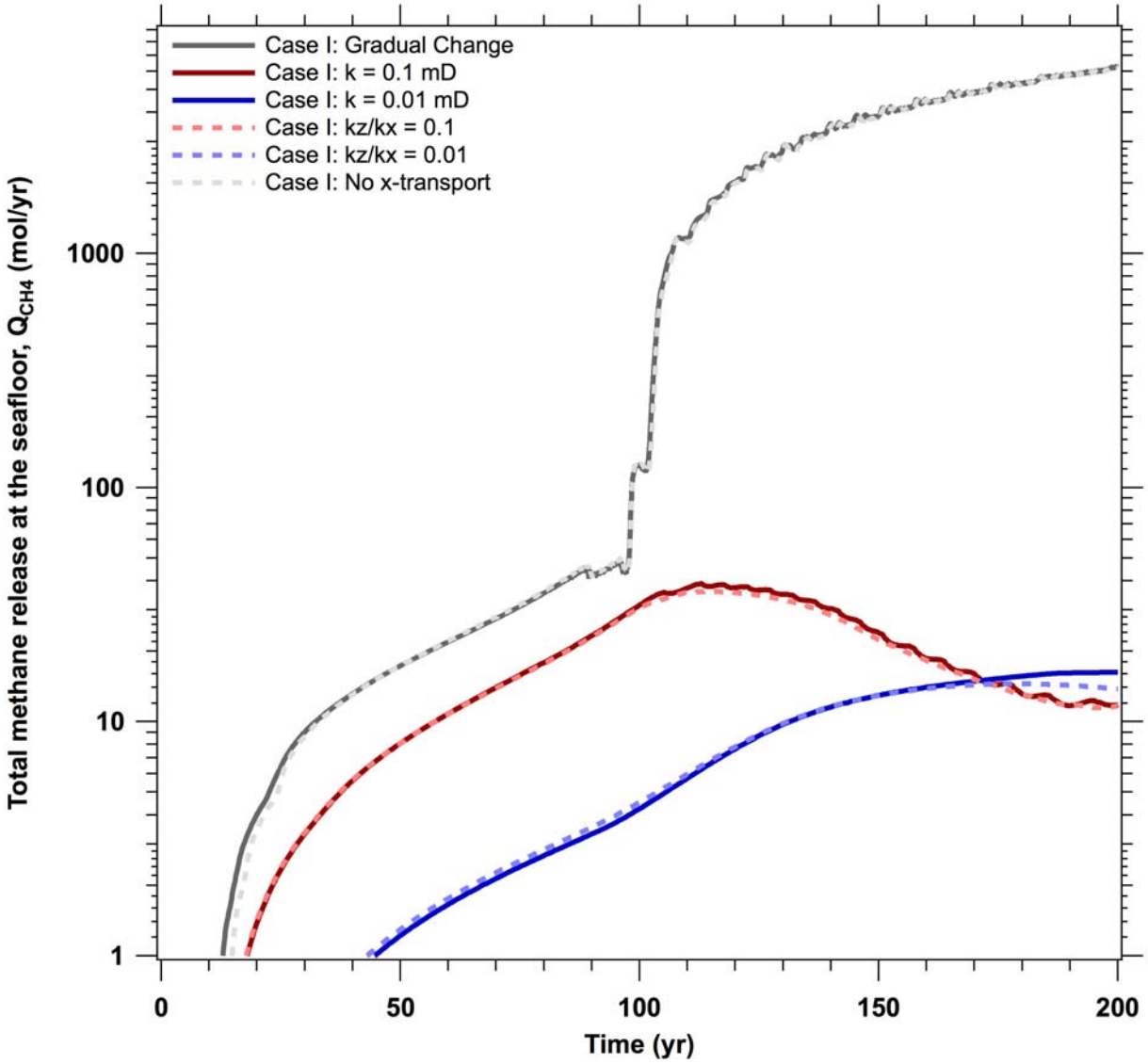

Figure 10. Variation of total methane release (aqueous and gaseous phases), $Q_{CH4,T}$ as a function of (Case I.1) permeability, (Case I.2) anisotropy, and (Case I.3) limited horizontal transport for Case I over the entire simulated seafloor boundary, a 1 m-wide, 5000 m long section.

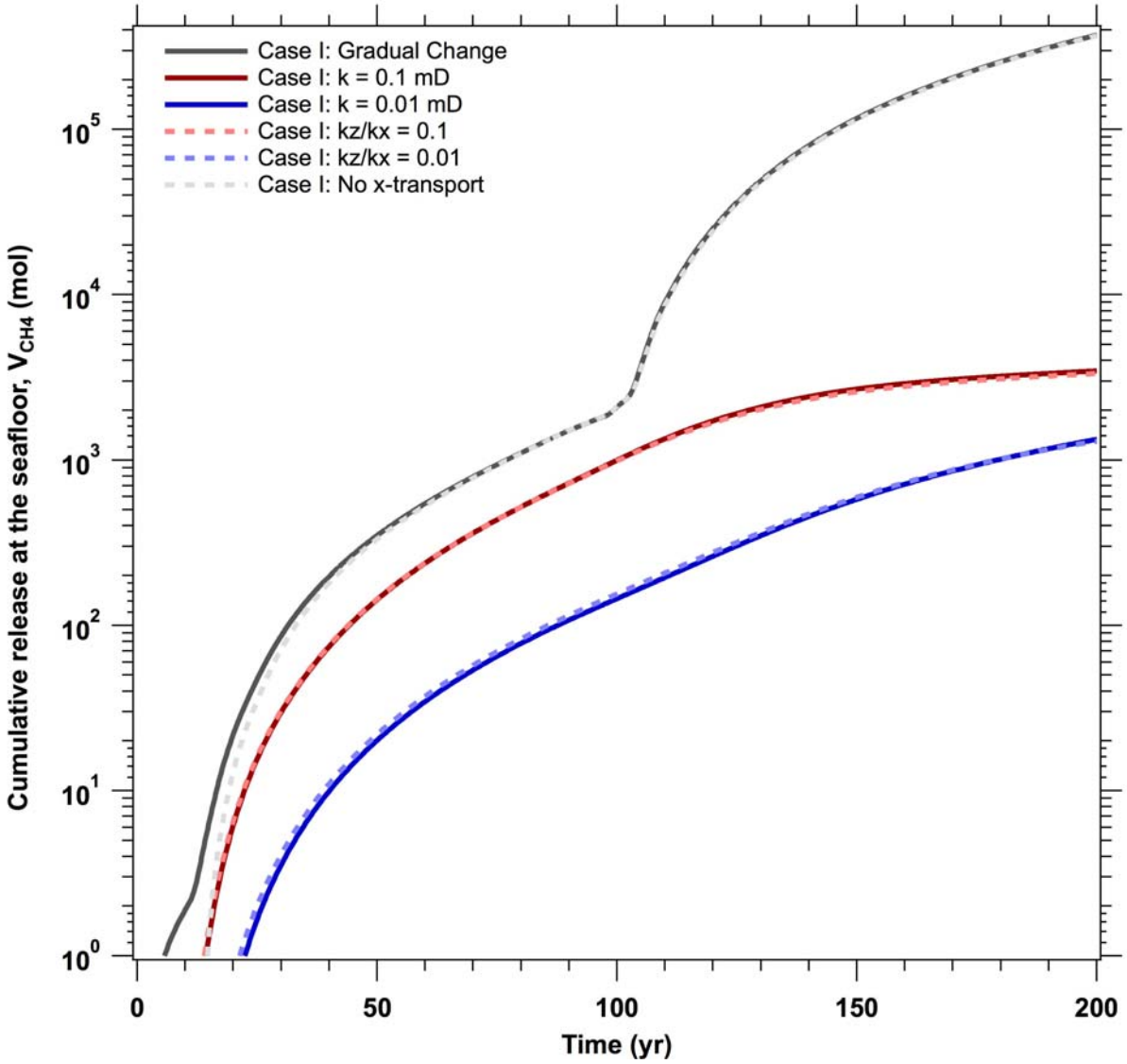

Figure 11. Variation of cumulative methane release (aqueous and gaseous phases), $V_{CH4,T}$ as a function of (Case I.1) permeability, (Case I.2) anisotropy, and (Case I.3) horizontal transport for Case I over the entire simulated seafloor boundary, a 1 m-wide, 5000 m long section.

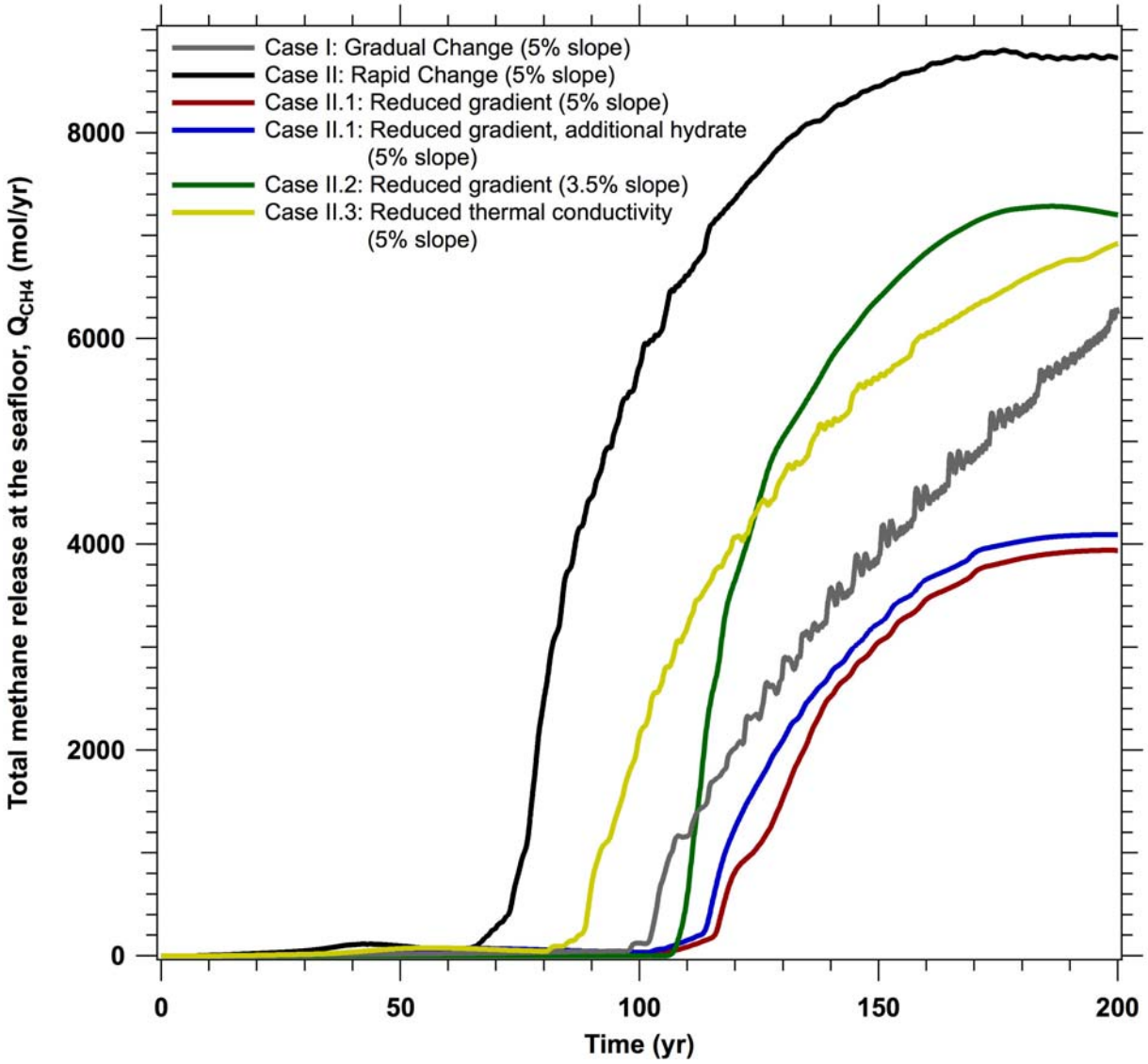

Figure 12. Variation of total methane release (aqueous and gaseous phases), $Q_{CH4,T}$ as a function of (II.1) decreased geothermal gradient, (II.1) the resulting change in GHSZ extent, (II.2) slope angle, and (II.3) sediment thermal conductivity for Case II over the entire simulated seafloor boundary, a 1 m-wide, 5000 m long section.

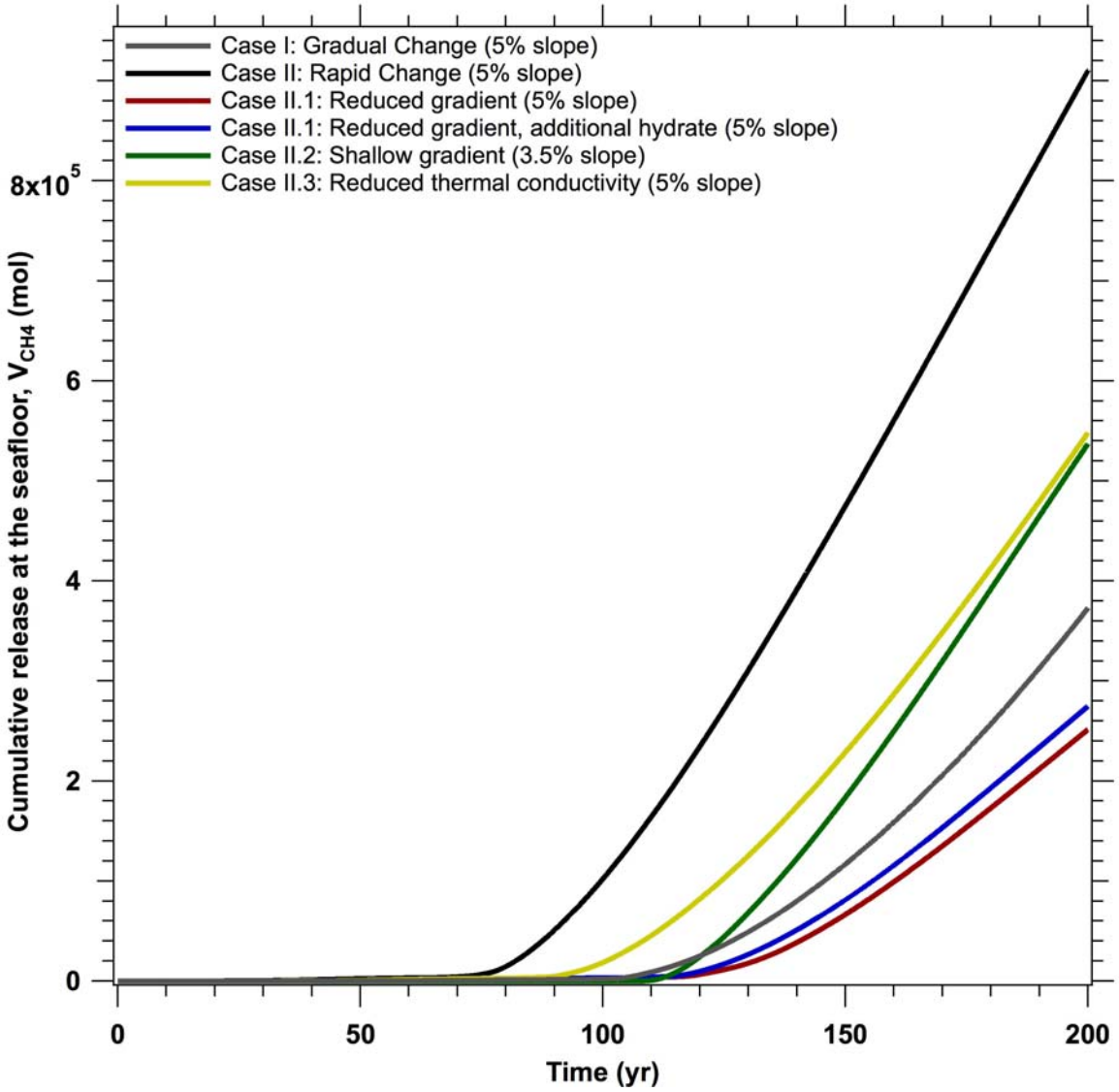

Figure 13. Variation of cumulative methane release (aqueous and gaseous phases), $V_{CH4,T}$ as a function of (II.1) decreased geothermal gradient, (II.1) the resulting change in GHSZ extent, (II.2) slope angle, and (II.3) sediment thermal conductivity for Case II over the entire simulated seafloor boundary, a 1 m-wide, 5000 m long section.